

3D Scene Creation and Rendering via Rough Meshes: A Lighting Transfer Avenue

Bowen Cai^{*,1}, Yujie Li^{*,1}, Yuqin Liang¹, Rongfei Jia¹, Binqiang Zhao¹, Mingming Gong², Huan Fu¹

Abstract—This paper studies how to flexibly integrate reconstructed 3D models into practical 3D modeling pipelines such as 3D scene creation and rendering. Due to the technical difficulty, one can only obtain rough 3D models (R3DMs) for most real objects using existing 3D reconstruction techniques. As a result, physically-based rendering (PBR) would render low-quality images or videos for scenes that are constructed by R3DMs. One promising solution would be representing real-world objects as Neural Fields such as NeRFs, which are able to generate photo-realistic renderings of an object under desired viewpoints. However, a drawback is that the synthesized views through Neural Fields Rendering (NFR) cannot reflect the simulated lighting details on R3DMs in PBR pipelines, especially when object interactions in the 3D scene creation cause local shadows. To solve this dilemma, we propose a lighting transfer network (LighTNet) to bridge NFR and PBR, such that they can benefit from each other. LighTNet reasons about a simplified image composition model, remedies the uneven surface issue caused by R3DMs, and is empowered by several perceptual-motivated constraints and a new Lab angle loss which enhances the contrast between lighting strength and colors. Comparisons demonstrate that LighTNet is superior in synthesizing impressive lighting, and is promising in pushing NFR further in practical 3D modeling workflows.

Index Terms—3D Scene Creation, Scene Synthesis, Lighting Transfer, Neural Rendering, Physically-based Rendering

1 INTRODUCTION

THE computer vision and graphics communities have put tremendous efforts into studying objects' representation methods for 3D modeling over the past years. In practical 3D modeling pipelines such as 3D scene designing, augmented reality (AR), and robotics, objects are usually represented as 3D CAD meshes combined with their materials and texture atlases (denoted as 3DMs). However, even the state-of-the-art (SOTA) 3D reconstruction methods do not have very accurate mesh reconstructions [1], [2], [3], [4], [5]. As a consequence, physical-based rendering (PBR) can only render low-quality content from these rough 3D models (R3DMs).

In this paper, we study how to flexibly integrate reconstructed 3D models into practical 3D modeling pipelines such as 3D scene creation and rendering. More specifically, we consider a practical setting in which one can utilize R3DMs (or R3DMs together with 3DMs) to create any scenes and assign arbitrary lighting to each created scene. Our goal is to render high-quality content from these possible scenes without training (or fitting) the newly created scenes. A possible solution is to represent real-world objects as *Neural Fields* such as NeRF [6] in addition to R3DMs. Specifically, in the design process, the primary role of a 3D model lies in interaction (with the environment and with light). If we can obtain information about these interactions (such as the effects of various lights on objects) through physical rendering, and then combine this with NeRF to acquire high-precision appearance information, we can use neural

networks to simulate the process of rendering element composition. This enables us to mitigate the impact of rough 3D models and obtain high-precision scene renderings. As shown in Fig. 1, given both the explicit representations (R3DMs) and implicit representations (NeRFs) of several real-world objects, artists can create unlimited 3D scenes in graphics software, then freely render high-quality images and videos by simply compositing PBR images and NFR images.

In further, artists may perform free lighting simulation to their created 3D scenes (*e.g.* setting several strong light sources) to capture realistic renderings. The remained question is that the above rendering routing cannot reflect the simulated lighting details on R3DMs in PBR pipelines, especially when object interactions in the 3D scene creation cause local shadows. Some works on neural light fields [7], [8], [9], [10], [11], [12] learn to simulate arbitrary lighting to an object or a scene. Still, they cannot model the complex local shadows without fitting a static scene under many possible lighting conditions. Thus, these light field methods would require training on each newly created scene under different lighting conditions, which is impractical for real-world applications.

To solve the dilemma, we propose a Lighting Transfer Network (LighTNet) to bridge NFR and PBR, such that they can benefit from each other. LighTNet takes “Shading” rendered from a PBR system and a synthesized image by NFR techniques (*e.g.* NeRF) as input and outputs photo-realistic renderings with rich lighting details. Taking inspiration from the image composition process in V-Ray [13], we prudently reformulate it to remedy the non-smooth “Shading” surfaces caused by R3DMs as well as better preserve lighting details. Furthermore, we propose perceptual-motivated constraints to optimize LighTNet and introduce a novel *Lab* Angle loss which can enhance the contrast

- Bowen Cai and Yujie Li contribute equally to this paper.
- 1. Tao Technology Department, Alibaba Group.
- 2. School of Mathematics and Statistics, The University of Melbourne.

Manuscript received April 19, 2005; revised August 26, 2015.

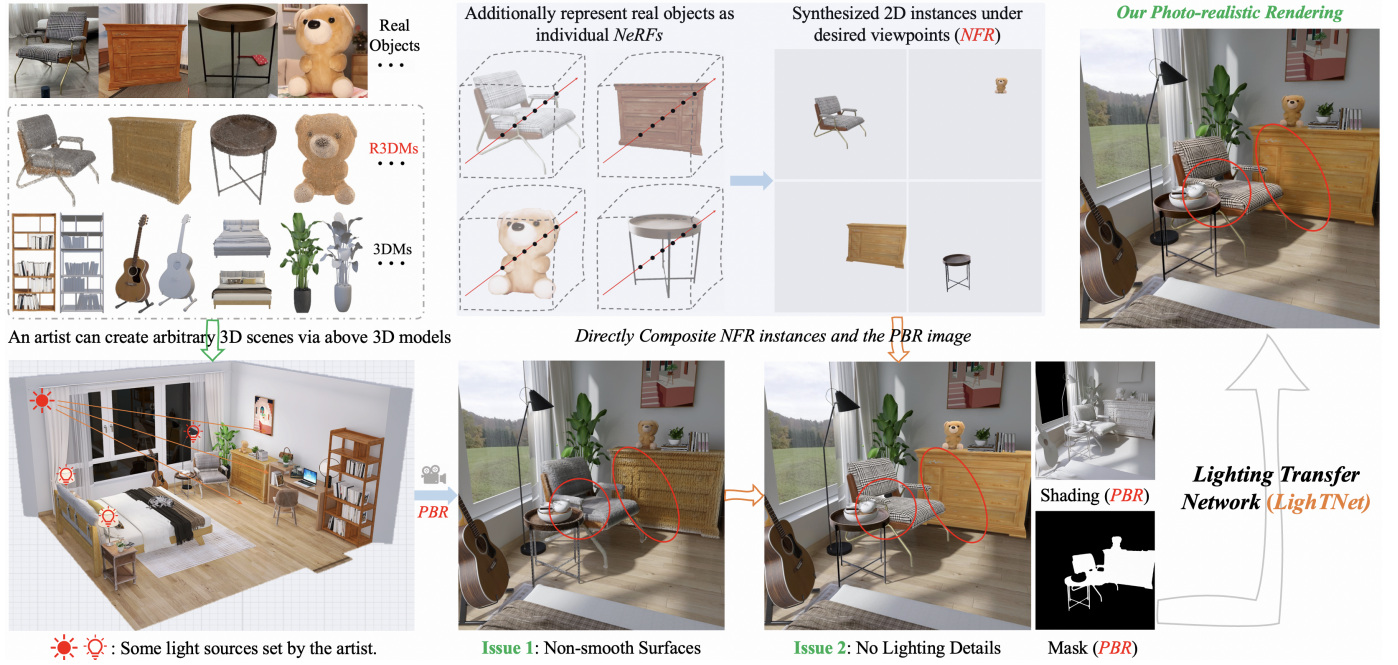


Fig. 1. **A Lighting Transfer Avenue.** *Left (Problem):* Given some reconstructed rough 3D models (R3DMs) and designed 3D CAD models (3DMs), artists can use them to create any 3D scenes and freely perform arbitrary lighting simulation for each created scene. A physically-based rendering (PBR) system can only render low-quality images or videos for these scenes. Our goal is to render high-quality content from these possible scenes without training (or fitting) the newly created 3D scenes. *Right (Solution):* As an example, if we have pre-obtained a neural fields representation (e.g. NeRF [6]) for each real object, we can synthesize object instances for R3DMs in impressive quality through neural fields rendering (NFR). Unluckily, NFR instances cannot reflect the simulated lighting details (e.g., local shadows) on R3DMs. We propose a lighting transfer network (LighTNet) to bridge NFR and PBR, such that they can benefit from each other. In practice, LighTNet is trained once in a dataset and can be used for all the newly created 3D scenes with both seen and unseen R3DMs and arbitrary lighting (See “Generalizing to Real-Lighting” in Fig. 11).

between lighting strength and colors. To train LighTNet, we synthesize R3DMs by injecting random noises into 3DMs and use these $\langle \text{R3DM}, \text{3DM} \rangle$ pairs as the training data. Once LighTNet is learned on the training data, it can be used for arbitrarily newly created 3D scenes with both seen and unseen R3DMs. Experiments show that LighTNet is superior in synthesizing impressive lighting details.

In summary, our main contributions are as follows:

- We present a lighting transfer avenue that allows artists to create arbitrary 3D scenes, flexibly simulate lighting, and freely render photo-realistic images and videos via R3DMs and 3DMs in any graphic software.
- With the pathway, we develop a lighting transfer network (LighTNet) leveraging a prudently reformulated image composition formulation. This network effectively bridges the lighting gap between PBR and NFR, showing promise in addressing the non-smooth “Shading” surfaces resulting from R3DMs.
- We introduce a *Lab Angle* loss to enhance the contrast between lighting strength and colors which can further improve the rendering quality.

2 RELATED WORK

2.1 3D Object Reconstruction

Typical SFM and MVS approaches [14], [15], [16] can reconstruct 3D meshes of objects that are with rich textures in reasonable quality. Leveraging large database, researchers exploit deep neural networks to reconstruct point clouds

[17], [18], [19], [20], voxel grids [21], [22], [23], [24], [25], and meshes [26], [27], [28], [29] from single or multiple images. Other works show learning implicit representations for objects is a promising avenue [1], [2], [30], [31], [32], [33], [34], [35], [36]. For example, IDR [5] and DVR [4] take advantage of differentiable rendering formulation for implicit shape and texture representations and show the possibility of recovering smooth surfaces for objects with rich textures from a set of posed images. They cannot handle many real-world cases, such as big items with flattened areas (e.g. furniture). Besides, they fall into the neural rendering category, thus would also benefit from the lighting transfer avenue.

To the best of our knowledge, no high-performing solution can automatically reconstruct perfect meshes and their UV texture atlases for real-world objects. Moreover, even if we can obtain an ideal 3D model with a perfect topology, we also need to rebuild its UV textures and materials. Unfortunately, texture and material recovery are currently receiving relatively poor attention, and the progress is not smooth.

2.2 Neural Rendering Leveraging NeRFs

Recent advances show neural fields representations are promising to describe scenes, and support rendering photo-realistic images of the fitted scenes under desired viewpoints [6], [37], [39], [40], [41], [42], [43], [44], [45], [46], [47], [48], [49], [50], [51], [52]. Concurrently, MobileNeRF [37] has performed scene edition application by representing real-world objects as individual NeRFs and R3DMs. Meta in

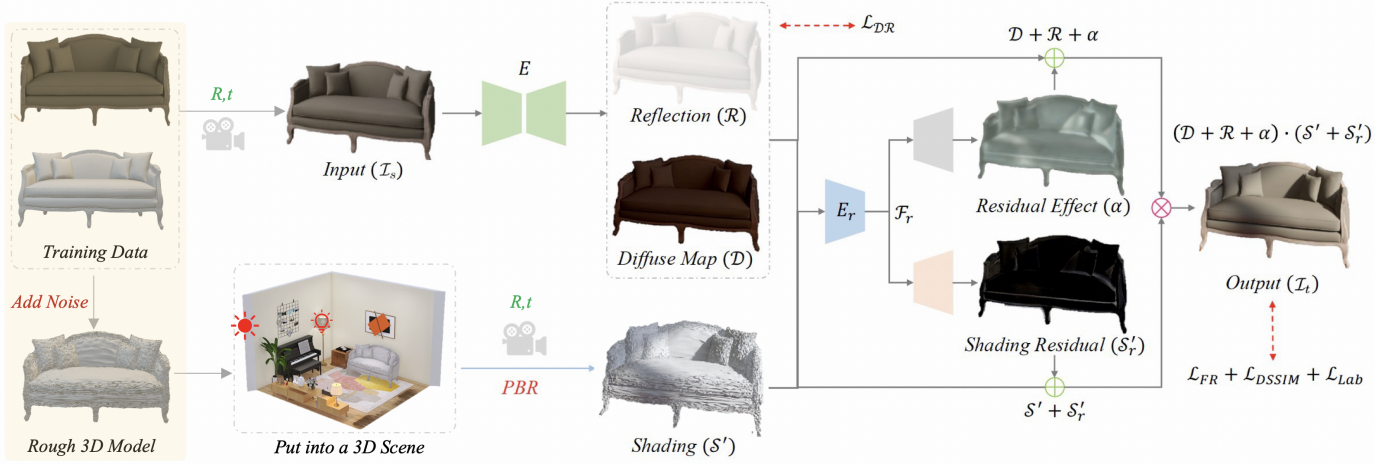


Fig. 2. **Training a LightNet.** LightNet aims to transfer the lighting details from an imperfect shading map S' to the corresponding image I_s . It reasons about the reformulated image composition model $I_t = (D + R + \alpha) \cdot (S' + S'_r)$. The yellow (left) part shows the $\langle R3DM, 3DM \rangle$ pairs generation process, and is only included in the training process. Once optimized, LightNet can be used for any newly created 3D scenes with both seen and unseen R3DMs and support free lighting simulation. In the inference phase, I_s of an object is the 2D instance synthesized by a trained NeRF or any other high-performing free view synthesis formulations (See Fig. 1 and Fig. 4).



Fig. 3. **Compositing Individual NeRF Objects.** Several concurrent works [37], [38] show it's possible to represent real-world objects as individual NeRFs and R3DMs for freely 3D scene creation and rendering. LightNet goes a further step by considering the indirect lighting effects such as local shadows on R3DMs caused by objects interactions.

Meta Connect 2022 [38] demonstrates this routine supports direct shadow simulations. The proposed lighting transfer avenue goes a further step by modeling the indirect lighting effects, such as local shadows on R3DMs caused by object-to-object interactions.

There are several works [53], [54], [55] that have also exploited free scene lighting editing. Unlike these approaches that would first perform per-scene optimization before editing and rendering, LightNet is a generic solution that can be directly integrated into practical 3D modeling pipelines for scene creation and rendering without per-scene optimization. It's worth mentioning that some works study inverse rendering with implicit neural representations that enable material editing and free view relighting of their reconstructed scenes (or objects) [11], [56], [57], [58], [59]. Our setting is totally different from theirs. For example, they can only synthesize local shadows caused by *self-occlusion* of its optimized single scene (or object). In fact, they have not considered compositing individual NeRFs to freely create

and edit 3D scenes, thus have not handle the possible indirect lighting effects caused by objects interaction. We refer to the "Discussion" section for more explanation about the differences.

3 LIGHTING TRANSFER NETWORK (LIGHTNET)

As shown in Fig. 2, the goal of LightNet is to transfer the lighting details from an imperfect shading map S' to the corresponding image I_s . We will start with a brief introduction to the simplified image composition formulation in Sec. 3.1, which is the theoretical basis of LightNet. Then, we explain the network architecture in Sec. 3.2. Finally, in Sec. 3.3, we introduce the proposed *Lab Angle Loss* and other involved objectives.

Importantly, in Sec. 4, we will take a specific example to explain the *Lighting Transfer* avenue. We show how a trained LightNet allows us to flexibly create 3D scenes, edit lighting, and render high-quality images and videos via R3DMs and 3DMs.

3.1 Preliminaries: Image Composition

An image can be expressed as the point-wise product between its shading S and albedo \mathcal{A} , i.e., $I = \mathcal{A} \cdot S$, as discussed in [60], [61], [62], [63]. \mathcal{A} is often simplified as a diffuse map which shows the base colors and textures used in materials with no lighting information. However, the render equation [64] in general physically-based renders tells us \mathcal{A} should encode other material properties such as refraction and specularities. We follow the compositing process and definitions in V-Ray [13] and simplify its formulation as

$$I = D \cdot S + R \cdot R_l + \alpha_2, \quad (1)$$

where D is the diffuse map, S is all the raw lighting (both direct and indirect) in the scene and we regard it as "Shading" in this paper, R defines the strength of the reflection of the materials, R_l stores reflection information calculated from

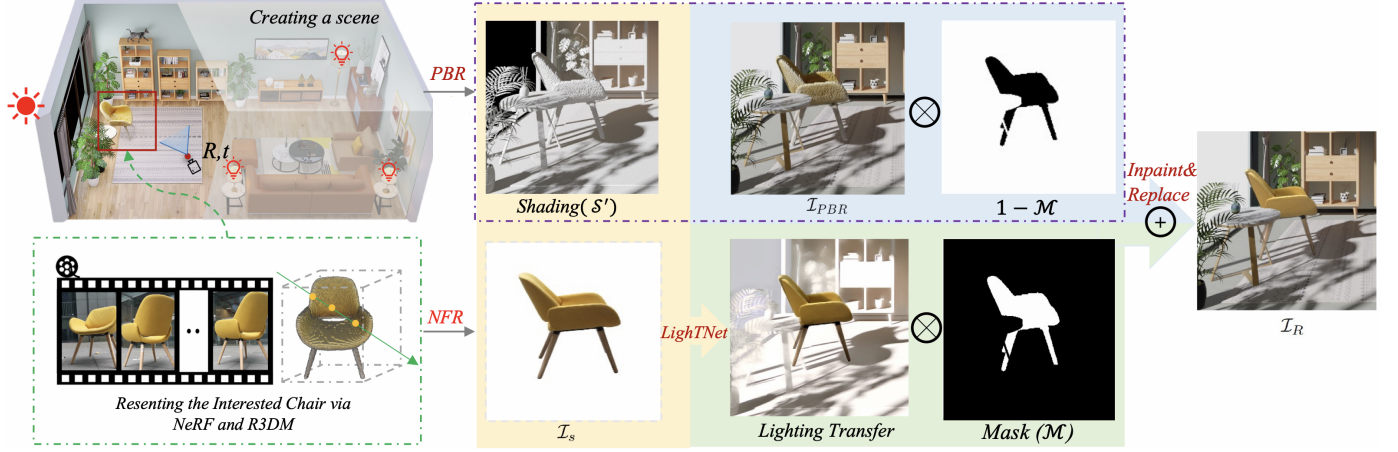


Fig. 4. **3D Scene Creation and Rendering via R3DMs.** We can represent real-world objects as individual NeRFs and R3DMs, and freely composite them to create unlimited 3D scenes. After lighting editing by artists, LightTNet can transfer direct and indirect lighting effects on R3DMs (e.g. S') to the corresponding NFR instances (e.g. I_s). See Sec. 4 for the detailed explanation.

the materials' reflection values in the scene, and α_2 provides the interactive effects between other material properties and lighting. As S encodes the per-pixel lighting of a scene, we approximate \mathcal{R}_l via $S + \alpha_1$. Going a further step, we find that rendering the supervision information $S + \alpha_1$ and α_2 is impractical because we only have a rough geometry R3DM. Besides, learning them separately would increase our framework complexity. We thus further simplify the formulation as

$$\mathcal{I} = (\mathcal{D} + \mathcal{R} + \alpha) \cdot S \quad (2)$$

by regarding $(\mathcal{R} \cdot \alpha_1 + \alpha_2)/S$ as a packed residual effect α .

3.2 Architecture

Our lighting transfer network (LightTNet) is developed based on the formulation $\mathcal{I} = (\mathcal{D} + \mathcal{R} + \alpha) \cdot S$. Given a training sample $(I_s, S', \bar{I}_t, \bar{\mathcal{D}}, \bar{\mathcal{R}})$, where \bar{I}_t , $\bar{\mathcal{D}}$, and $\bar{\mathcal{R}}$ are the ground-truth images, LightTNet takes I_s and S' as inputs, and target at reconstructing \bar{I}_t . See Sec. 5.1 for details about the training samples capturing process.

We utilize an encoder-decoder network E to estimate both the diffuse map \mathcal{D} and the reflection strength \mathcal{R} from I_s . We learn \mathcal{R} and \mathcal{D} in a supervised manner using:

$$\mathcal{L}_{\mathcal{DR}} = |\mathcal{R} - \bar{\mathcal{R}}| + |\mathcal{D} - \bar{\mathcal{D}}|. \quad (3)$$

After that, the remained major issue is that the shading S' is not smooth since its R3DM's surfaces are uneven. We know that shading is determined by surface normal and illumination [62]. We clarify \mathcal{D} and \mathcal{R} mapping from I_s usually imply smooth normal information that could remedy S' . Towards the purpose, we obtain an intermediate representation by concatenating S' , \mathcal{D} , and \mathcal{R} together, and take an encoder network (E_r) to map it to a feature \mathcal{F}_r . With \mathcal{F}_r , a straightforward option is to directly predict a smooth shading S . In our experiments, we find a smoother S could be captured following $S = S' + S'_r$, where S'_r is the learned residual from \mathcal{F}_r via a decoder network ($D_{S'}$).

Finally, as analyzed before, the model $\mathcal{I} = (\mathcal{D} + \mathcal{R}) \cdot S$ cannot describe the full lighting effects. Especially, our experiments in Fig. 7 show it cannot well preserve shadows.

We thus follow Eqn. 2 to directly predict a residual effect α from \mathcal{F}_r through another decoder network (D_α). Considering all above, the target image can be composited as

$$I_t = (\mathcal{D} + \mathcal{R} + \alpha) \cdot (S' + S'_r). \quad (4)$$

3.3 Objectives

In previous relighting efforts, the $L1$ photometric loss \mathcal{L}_{L1} ($|I_t - \bar{I}_t|$ or $|\log I_t - \log \bar{I}_t|$) was commonly used as a major term to preserve the basic image content in the reconstruction process [66], [67], [68]. However, we find in our experiments it will degrade the lighting transfer ability of LightTNet as shown in Fig. 9. A possible reason is that it pushes the learning procedure to focus more on reducing the color differences instead of local lighting discrepancies. We thus propose to minimize the following losses that are closely related to perceptual quality and lighting effects.

Feature Reconstruction Loss. The feature reconstitution loss [69] encourages I_t to be perceptually similar to \bar{I}_t by matching their semantic features. We take VGG-19 [70] pretrained on ImageNet [71] as the feature extractor ϕ and denote $\phi_j(x)$ as the output of the j th convolution block. The feature reconstruction loss is expressed as:

$$\mathcal{L}_{FR} = \frac{1}{C_j * H_j * W_j} \sum_{c,h,w} \|\phi_j(I_t) - \phi_j(\bar{I}_t)\|, \quad (5)$$

where $C_j * H_j * W_j$ is the feature dimensions of $\phi_j(x)$. In this paper, we utilize activations of the third convolution block ($j = 3$) to compute \mathcal{L}_{FR} .

Structural Dissimilarity. SSIM [72] is another perceptual-motivated metric that measures structural similarity between two images. We take the structural dissimilarity (DSSIM) as a measure following the success in [73]:

$$\mathcal{L}_{DSSIM} = \frac{1 - \text{SSIM}(I_t, \bar{I}_t)}{2}, \quad (6)$$

Lab Angle Loss. We find that LightTNet optimized with aforementioned loss terms would produce images with



Fig. 5. **Training Set Construction.** We take the ‘‘Sofa’’ case as an example to show how to capture a training sample $\{(\mathcal{I}_s, \mathcal{S}', \bar{\mathcal{I}}_t, \bar{\mathcal{D}}, \bar{\mathcal{R}})\}$ via 3D CAD models and 3D scenes. The elements are rendered by Blender [65]. LightNet is trained once on the 3DF-Lighting training set, and can be used for all the newly created scenes with both seen and unseen R3DMs and arbitrary lighting.

darker global brightness as shown in Fig. 9. A possible reason is that \mathcal{L}_{FR} and \mathcal{L}_{DSSIM} only enhance local perceptual quality while overlooking the lighting contrast. In the paper, we thus propose a novel *Lab* Angle loss to consider the pixel-wise ratio between lighting strength and colors as:

$$\mathcal{L}_{Lab} = \frac{1}{H * W} \sum_{h,w} \arccos \left(\frac{\langle \varphi(\mathcal{I}_t)_{(h,w)}, \varphi(\bar{\mathcal{I}}_t)_{(h,w)} \rangle}{\|\langle \varphi(\mathcal{I}_t)_{(h,w)}, \varphi(\bar{\mathcal{I}}_t)_{(h,w)} \rangle\|} \right), \quad (7)$$

where $\langle x, y \rangle$ denotes the inner product of vector x and y , $\varphi(\cdot)$ represents the *RGB* to *Lab* converter, (h, w) is the spatial location, and $H * W$ is the image size.

Full Objective. Our LightNet is optimized in an end-to-end fashion with the objective:

$$\mathcal{L} = \mathcal{L}_{DR} + \lambda_1 \mathcal{L}_{FR} + \lambda_2 \mathcal{L}_{DSSIM} + \lambda_3 \mathcal{L}_{Lab}, \quad (8)$$

where the loss weights λ_1 , λ_2 , and λ_3 , in all the experiments, are set to 0.05, 0.5, and 0.5, respectively.

4 RENDERING WITH LIGHTNET AND R3DMs

In this section, we show how a trained LightNet and R3DMs can be flexibly integrated into practical 3D modeling workflows such as 3D scene creation and rendering. For example, we are interested in a real yellow chair, as shown in Fig. 4. Given its reconstructed R3DM and neural fields representation (NeRF [6] in this paper), we can create a 3D scene by putting the yellow chair’s R3DM and some 3DMs into a 3D room. Here, both the room and the involved 3DMs have not been seen before. To showcase the scene, we would like to render a high-quality image, in which the involved 3D models are with rich lighting details. Towards the goal, we can set a high-energy light source, and render a scene image \mathcal{I}_{PBR} , a shading \mathcal{S}' , and an object’s mask \mathcal{M} , under a good viewpoint. Simultaneously, we synthesize an image \mathcal{I}_s with the same camera pose via NeRF. Then, we are able to capture a target image \mathcal{I}_t by transferring lighting from $\mathcal{S}' \cdot \mathcal{M}$

TABLE 1
Quantitative Evaluation on 3DF-Lighting. We use the proposed *Lab* Angle distance and several widely studied metrics, including *L1*-Norm, PSNR, and SSIM [72], to measure a method’s lighting transfer ability. LightNet and LightNet[†] denote training LightNet with Blender and NeRF images, respectively (Refer to Sec. 5.1.1).

Method	<i>L1</i> -Norm ↓	PSNR ↑	SSIM ↑	<i>Lab</i> Angle ↓
Pix2Pix [75]	0.0345	26.65	0.9042	0.4314
DPR [76]	0.0399	25.39	0.8692	0.4576
SSVBRDF [68]	0.0373	26.02	0.9040	0.3796
LightNet	0.0219	30.17	0.9142	0.3137
LightNet [†]	0.0281	29.93	0.9203	0.3173

to $\mathcal{I}_s \cdot \mathcal{M}$ via the trained LightNet model. Finally, we replace $\mathcal{I}_{PBR} \cdot \mathcal{M}$ with $\mathcal{I}_t \cdot \mathcal{M}$ to obtain the final photo-realistic rendering \mathcal{I}_R . The complete process can be formulated as:

$$\mathcal{I}_R = \mathcal{I}_{PBR} \otimes (1 - \mathcal{M}) + \mathcal{M} \otimes \text{LightNet}(\mathcal{I}_s, \mathcal{S}'), \quad (9)$$

where \otimes is the element-wise production operation. In practice, there will be some regions in boundary areas that cannot be covered by \mathcal{I}_t . We directly fill these regions via a SOTA image inpainting technique [74]. Some qualitative results are shown in Fig. 11.

5 EXPERIMENTS

In this section, we conduct many experiments to examine the lighting transfer avenue. We first present the training and evaluation sets building processes in Sec. 5.1. Then, we build several baselines and make benchmark comparisons with them in Sec. 5.2. Finally, we perform various ablation studies to discuss our method in Sec. 5.3.

5.1 Datasets

5.1.1 3DF-Lighting

Training Set: We take 50 3D scenes and the involved 30 3D CAD models (denoted as 3DMs) in 3D-FRONT [77] to

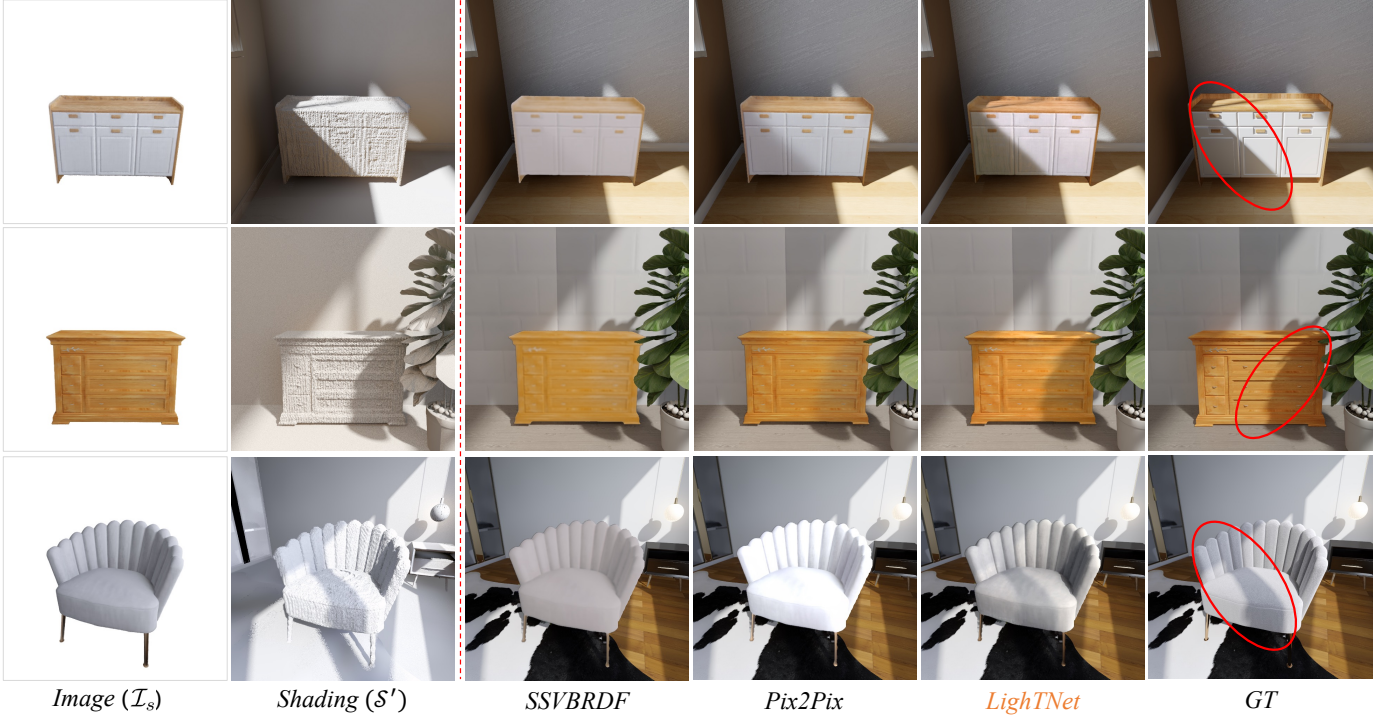


Fig. 6. **Qualitative Comparisons on 3DF-Lighting.** We make qualitative comparisons with the reformulated Pix2Pix [75] and SSVBRDF [68]. LightTNet achieves realistic relighting results with impressive shadow details. \mathcal{I}_s and \mathcal{S}' are rendered by NFR and PBR, respectively.

construct the training set. First, we need to recover these objects' rough 3D meshes (R3DMs). We simply adopt the mesh subdivision algorithm [78], [79] to densify the CAD models' surfaces, then add random noise to each vertex. Second, for a specific object in a scene, we simulate uniform sunlight to the scene, randomly choose a viewpoint and render the object's diffuse map $\bar{\mathcal{D}}$, reflection strength $\bar{\mathcal{R}}$, and color image \mathcal{I}_s . Third, we randomly change the light source's position and increase the lighting energy to capture a target image $\bar{\mathcal{I}}_t$. Finally, we render the rough shading \mathcal{S}' by replacing the object's 3DM as its R3DM. Following the pipeline, we can construct a training set $\{(\mathcal{I}_s, \mathcal{S}', \bar{\mathcal{I}}_t, \bar{\mathcal{D}}, \bar{\mathcal{R}})\}$. This paper takes Blender [65] with V-Ray plug-in as the render engine to secure these elements. We have also rendered \mathcal{I}_s to maintain consistency between training and inference. As reported in Tab. 1, the "NeRF" setting (LightTNet[†]) yields similar scores compared to the "Blender" setting (LightTNet).

Evaluation Set: We build a test set using another 10 furniture shapes and 20 3D scenes from 3D-FRONT. We take one object as an example to present the test set building process. We randomly render 200 images from viewpoints sampled on a full sphere to learn its NeRF and R3DM. For each 3D scene, we put the object's R3DM into the scene and randomly render thirty \mathcal{S}' and \mathcal{M} . Simultaneously, we synthesize the corresponding thirty \mathcal{I}_s using its NeRF. Finally, we render the thirty $\bar{\mathcal{I}}_t$ (ground truth images) at size 800×800 by replacing the R3DM with its 3DM. Each 3D scene's light source and energy are pre-defined. Through the workflow, we construct a test set with 6,000 samples $\{(\mathcal{I}_s, \mathcal{S}', \bar{\mathcal{I}}_t, \mathcal{M})\}$. We pre-assign V-Ray materials to each 3D model (R3DM and R3D) manually.

5.1.2 Generalizing to Real-Lighting

We also conduct qualitative evaluation on a real dataset named Real-Lighting. Specifically, we capture some object-centric videos via a mobile phone, and reconstruct these objects via NeRF. We create some 3D scenes using these objects' R3DMs and other 3DMs. Some rendered images of these scenes are presented in Fig. 11. We can see the lighting details have been successfully preserved. The LightTNet model is trained only on the 3DF-Lighting train set. All the scenes and objects in Real-Lighting have not been seen previously.

Moreover, we choose two individuals from the ActorSHQ [80] dataset and incorporate two real-world 360 scenes from Mip-NeRF 360 [51] for our experiment. Using Instant-NGP [81], we reconstructed the two individuals, and for the two scenes, we employed Mip-NeRF 360 [51]. Subsequently, we integrated the digital representations of the individuals and objects into the reconstructed 3D scenes, forming new composite 3D scenes. Light sources were randomly placed in these new 3D scenes. That means, all the content in the new scenes are reconstructed. The qualitative results, depicted in Fig. 12 and the accompanying video, highlight the adaptability of our method to both human subjects and reconstructed real-world 3D scenes.

5.2 Benchmark Comparisons

Building Baselines. We build baselines by reformulating three works, including Pix2Pix [75], DPR [76], and SSVBRDF [68], to study the lighting transfer setting. Our research addresses a novel problem arising from the practical 3D house design and rendering workflow. With the proposed lighting transfer pathway depicted

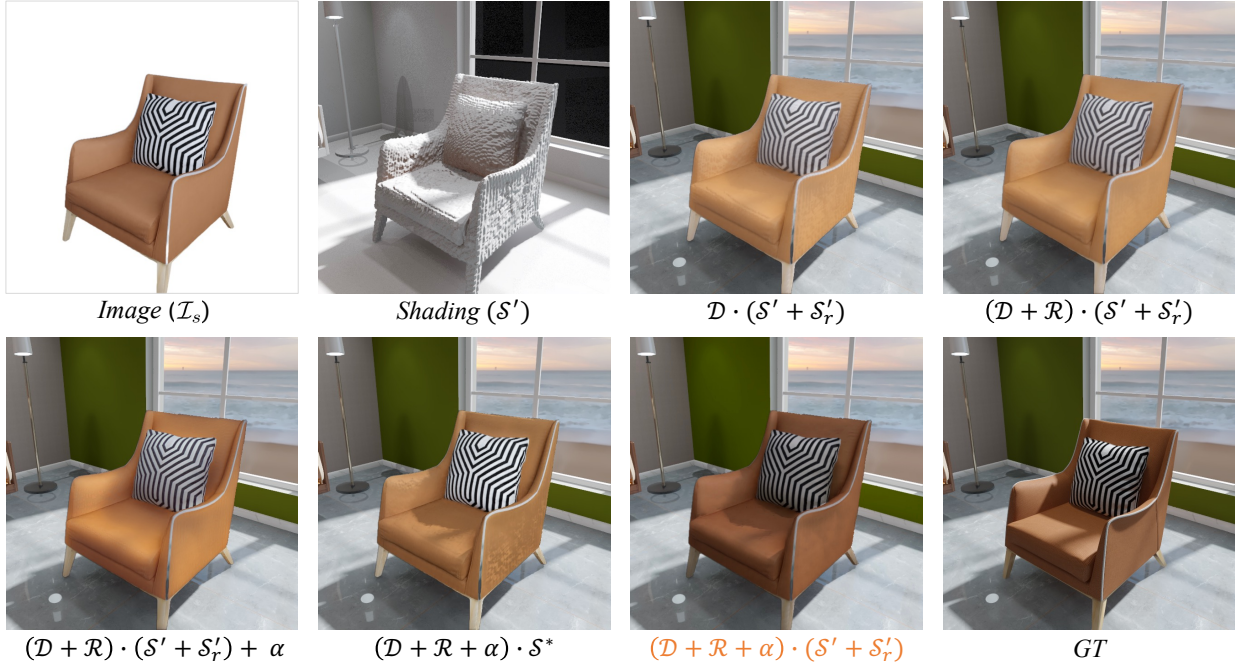


Fig. 7. We qualitatively evaluate the lighting transfer ability of the image composition variants. $(D + R + \alpha) \cdot S$ would be a much better choice for simulating the PBR compositing process.

TABLE 2
We find that optimizing LightNet with a $L1$ photometric loss ($\mathcal{L}_{L1} = |\mathcal{I}_t - \bar{\mathcal{I}}_t|$) would yield a degenerate performance.

Objective				Metric			
\mathcal{L}_{FR}	\mathcal{L}_{DSSIM}	\mathcal{L}_{Lab}	\mathcal{L}_{L1}	$L1$ -Norm ↓	PSNR ↑	SSIM ↑	Lab Angle ↓
			✓	0.0277	28.37	0.8774	0.3551
✓				0.0254	29.06	0.9006	0.3717
✓	✓			0.0229	29.83	0.9129	0.3317
✓	✓	✓		0.0219	30.17	0.9142	0.3137
✓	✓	✓	✓	0.0240	29.37	0.9102	0.3426

in Fig. 1, our objective is to transfer lighting details from the “Shading” map (S') to the NeRF rendering (\mathcal{I}_s) (refer to Fig. 4). While we accomplish this task through an image composition formulation based on the V-Ray render engine’s compositing process, it can also be viewed as a conditional image-to-image translation problem. Hence, Pix2Pix [75] is selected as one of our baselines. We learn the mapping from $\mathcal{I}_s \oplus S'$ to \mathcal{I}_t , where \oplus is the concatenate operation along the channel dimension. Considering DPR [76] and SSVBRDF [68], they belong to the realm of inverse rendering, predicting BRDF from single images and supporting image relighting. To decompose BRDF, they require predicting lighting (usually environment lighting or spherical harmonics) for a given single image. Consequently, we can integrate them into the proposed lighting transfer avenue by directly rendering the scenes’ spherical harmonics lighting through PBR and using it directly in the relighting process. All the methods (including LightNet) have been trained on the 3DF-Lighting train set.

Performance. To measure the lighting synthesis ability, we take $L1$ -Norm, PSNR, SSIM [72], and our Lab Angle loss as

the metrics. From the scores presented in Table 1, our LightNet outperforms the compared methods by a large margin. Especially, while the best PSNR and $L1$ -Norm obtained by the baselines are 26.65 and 0.0345, LightNet significantly improves them to 30.17 and 0.0219. It is not surprising since (1) DPR and SSVBRDF focus more on modeling global illumination, and (2) transferring lighting from shading with uneven surfaces is more challenging. Several qualitative comparisons are reported in Fig. 6. LightNet achieves realistic relighting results with impressive shadow details. In Fig. 11, we illustrate some further examples of our approach generalizing to real objects, using the LightNet model only trained on 3DF-Lighting.

5.3 Ablation Studies

We argue that a slight numerical gain over the studied metrics may imply an improved visual experience since lighting is a detailed effect. We refer to the supplemental material for more qualitative comparisons.

Objectives. We discuss the objectives presented in Sec. 3.3 based on our lighting transfer formulation Eqn. 4. We take

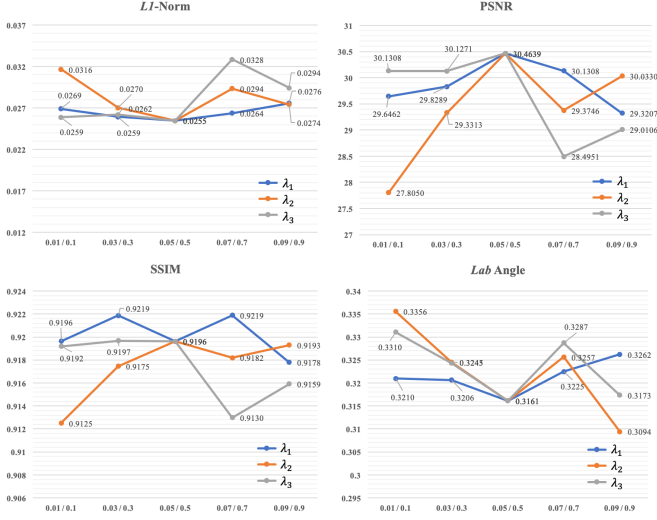


Fig. 8. **Weights for loss terms.** We study $\lambda_1 \mathcal{L}_{FR} + \lambda_2 \mathcal{L}_{DSSIM} + \lambda_3 \mathcal{L}_{Lab}$ through a controlled variable technique. See Sec. 5.3 for the setting of this ablation study.

\mathcal{L}_{FR} as the baseline, and incorporate other objectives one by one. \mathcal{L}_{DR} is used in all the experiments. From Table 2, there is a remarkable gap between \mathcal{L}_{L1} and \mathcal{L}_{FR} . Bringing in \mathcal{L}_{DSSIM} yields a notable improvement over all the metrics. In further, although \mathcal{L}_{Lab} only provides a slight PSNR gain (+0.34), it does enhance the lighting effects as reported in Fig. 9. It is worth mentioning that optimizing LightNet with an auxiliary \mathcal{L}_{L1} loss would largely degrade L1-Norm (−0.021) and PSNR (−0.8). See Fig. 9 for a qualitative evaluation.

Image Composition Formulations. In Table 3 (Top), we study the image composition variants discussed in Sec. 3.1. Overall, our revised formulation $(\mathcal{D} + \mathcal{R} + \alpha) \cdot \mathcal{S}$ outperforms the baseline $\mathcal{D} \cdot \mathcal{S}$ by a significant margin. From the first three columns, while \mathcal{R} supplements reflection effects, the residual α is important in encoding other lighting effects. By investigating $(\mathcal{D} + \mathcal{R} + \alpha) \cdot \mathcal{S}$ vs. $(\mathcal{D} + \mathcal{R}) \cdot \mathcal{S} + \alpha$, we find that it would be much better to simulate the PBR compositing process following the product manner. Some qualitative comparisons are shown in Fig. 7.

Learning \mathcal{S}'_r or Not? In Eqn. 4, we choose to learn a residual \mathcal{S}'_r to remedy the uneven surfaces of \mathcal{S}' . There is an alternative that directly estimates a smooth shading \mathcal{S}^* from \mathcal{F}_r . As presented in Table 3 (Bottom), while $(\mathcal{D} + \mathcal{R} + \alpha) \cdot \mathcal{S}^*$ improves $(\mathcal{D} + \mathcal{R} + \alpha) \cdot \mathcal{S}'$ by 0.65 on PSNR, our residual architecture significantly yields a PSNR gain of 1.47.

Smoothness of R3DMs. In Fig. 10, we explore the impact of the smoothness of R3DMs on the final rendering quality. It is not supersizing that if a method can recover smoother surfaces (e.g., NeuS), LightNet would perform better. For the “extremely noisy surfaces” case, LightNet fails to render the lighting details and cannot address the uneven artifacts. The reasons are: (1) a PBR system cannot produce a correct shading map for extremely noisy meshes, as the lighting effects are closely related to surface normals; (2)

TABLE 3

Image Composition Formulations. See Sec. 3.1 and Sec. 3.2 for explanations of these formulations. \mathcal{S}^* means that we directly predict a smooth shading from \mathcal{F}_r instead of estimating the shading residual \mathcal{S}'_r .

Variant	$L1\text{-Norm} \downarrow$	$PSNR \uparrow$	$SSIM \uparrow$	$Lab \text{ Angle} \downarrow$
Composition Formulations ($\mathcal{S} = \mathcal{S}' + \mathcal{S}'_r$)				
$\mathcal{D} \cdot \mathcal{S}$	0.0283	28.46	0.9128	0.3449
$(\mathcal{D} + \mathcal{R}) \cdot \mathcal{S}$	0.0262	28.83	0.9117	0.3411
$(\mathcal{D} + \mathcal{R}) \cdot \mathcal{S} + \alpha$	0.0238	29.45	0.9040	0.3458
$(\mathcal{D} + \mathcal{R} + \alpha) \cdot \mathcal{S}$	0.0219	30.17	0.9142	0.3137
Architecture: Learning \mathcal{S}'_r or Not				
$(\mathcal{D} + \mathcal{R} + \alpha) \cdot \mathcal{S}'$	0.0260	28.70	0.8935	0.3574
$(\mathcal{D} + \mathcal{R} + \alpha) \cdot \mathcal{S}^*$	0.0241	29.35	0.8996	0.3473
$(\mathcal{D} + \mathcal{R} + \alpha) \cdot (\mathcal{S}' + \mathcal{S}'_r)$	0.0219	30.17	0.9142	0.3137

The capability of LightNet is not sufficient to remedy these very worse typologies.

Weights for Loss Terms. Here, we simply study $\lambda_1 \mathcal{L}_{FR} + \lambda_2 \mathcal{L}_{DSSIM} + \lambda_3 \mathcal{L}_{Lab}$ through a controlled variable technique. The scores are reported in Fig. 8. For efficiency, this ablation was performed on a reduced subset (1/5) of 3DF-Lighting.

6 DISCUSSION

Setting. Our primary insight of develop such a lighting transfer avenue is inspired by the industry production pipeline. For example, in order to showcase furniture online, a furniture seller typically needs artists to reconstruct 3D CAD models of their furniture. Subsequently, designers use these 3D furniture models to create a virtual 3D CAD scene, and a rendering engine is employed to generate images and videos that effectively showcase the furniture. Crafting high-quality 3D furniture models is a costly endeavor, especially when dealing with unique materials or styles. Moreover, achieving high-quality furniture reconstructions requires the expertise of professional artists. With the motivation, we focus on how to flexibly integrate automatically reconstructed 3D models into practical 3D modeling workflows. Essentially, with the proposed lighting transfer avenue, one can import newly reconstructed Rough 3D Models (R3DMs) into graphical software (e.g., 3DS-Max). This allows users to design diverse indoor and outdoor 3D scenes and collaboratively render content alongside other high-quality 3D CAD models (3DMs). It’s noteworthy that NeRF in our paper serves as a specific example to illustrate the potential of the lighting transfer avenue. In our approach, the R3DM component is independent of the Neural Fields Rendering (NFR) synthesis (or NeRF) segment. For a real object, we can employ one method to reconstruct its R3DM and another method for 2D instance synthesis if it outperforms NeRF in novel view synthesis.

Relation to Inverse Rendering with Implicit Neural Representation. Leveraging implicit neural representation, recent inverse rendering works can decompose a scene under complex and unknown illumination into spatially varying

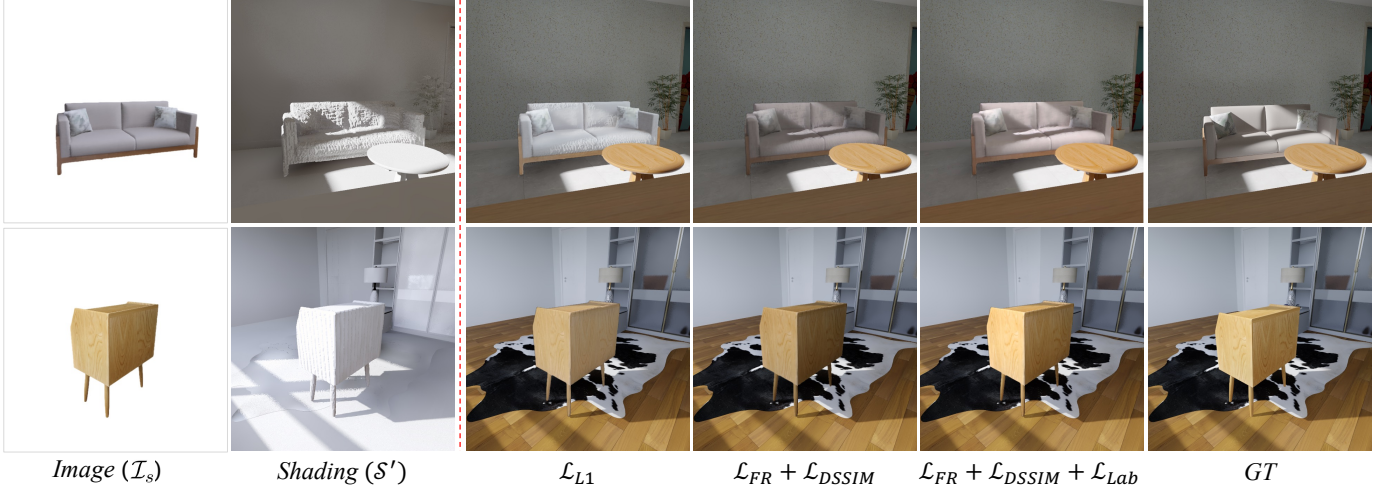


Fig. 9. We qualitatively discuss the objectives in Sec. 3.3. $\mathcal{L}_{FR} + \mathcal{L}_{DSSIM}$ yields a notable improvement in dealing with uneven shading surface and local shadows compared to \mathcal{L}_{L1} . \mathcal{L}_{Lab} could further enhance the lighting effects.

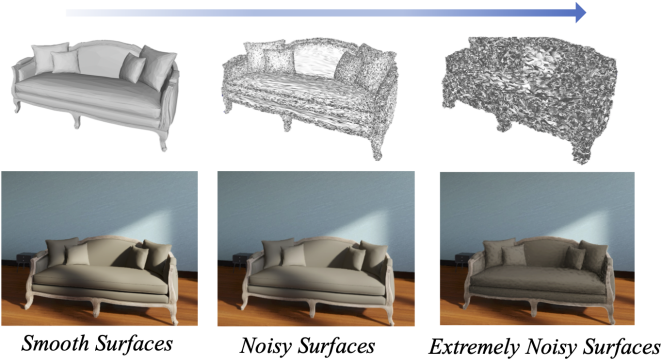


Fig. 10. **Smoothness of R3DMs.** We simulate different levels of noises to the sofa's 3D CAD model. See Sec. 5.1.1 for how to add geometry noise to 3DMs.

BRDF material properties [11], [56], [57], [58], [59]. These techniques enable material editing and free view relighting of the reconstructed scene. Here, we take NeRFactor [12] as an example to discuss the main differences of these works and the raised lighting transfer avenue. First, NeRFactor focused on estimate SVBRDF properties of single scene or object. Beyond free-view relighting, we can imagine that NeRFactor supports the object inserting application, *i.e.*, inserting a 3D object into a *static image*, as we can extract the global lighting probes from the target static image. But if we would like to insert multiple 3D objects into a single image, NeRFactor would overlook the possible indirect lighting effects caused by object-to-object occlusion because there is no a "3D scene" concept involved. It's worth mentioning NeRFactor can simulate local shadows caused by self-occlusion of its reconstructed single object. In contrast, we study a more practical problem that is "can we use rough 3D models, together with 3D CAD models drawing by artists, to create arbitrary 3D scenes and render high-quality contents?". Thereby, our studied setting is totally different from the setting of NeRFactor. Second, in the proposed lighting transfer avenue, the R3DM part is independent with the NFR synthesis part. For a real object, we can use a

method to reconstruct its R3DM, and use another method to perform 2D instance synthesizing. This paper takes NeRF as an example to explain the proposed avenue because: (1) it supports high-quality novel view synthesis; and (2) at the same time, we can conveniently extract a R3DM from a trained NeRF via a marching cube algorithm. From this perspective, we can apply NeRFactor instead of NeRF for 2D instance synthesizing. But as analyzed before, how should we handle the indirect lighting details caused by the interaction of multiple 3D objects? The introduced LightNet could give a possible answer to this question.

7 LIMITATION

Tough Materials. LightNet cannot handle strong specular materials yet. As shown in Fig. 13, the synthesized 2D instances by NeRF contain the reflected content. It's unavoidable yet as NeRF series learn to fit a *captured scene* for its free view synthesis. We find LightNet would preserve the reflected content while ignoring the real reflected content of the newly created scenes. A possible reason is that we do not have strong specular materials in our training set, as 3D-FRONT only shared several specular objects. It should be one of the major limitations. This issue would disappear if future NeRF research or other view synthesis works can disentangle the reflected content from the objects' textures. Moreover, our approach struggles with scattering materials (e.g., clouds) and objects with intricate structures (e.g., Eiffel Tower). The current methodology falls short in recovering the meaningful geometry of these categories, resulting in a "Shading" map riddled with considerable noise.

Blurriness & Dark spots. Our renderings exhibit slight blurriness compared to ground truth (GT) images and contain artifacts such as dark spots. Regarding the blurriness, it's reasonable to expect that images generated by a standard CNN, like our composition network, may not seamlessly match the quality of those rendered by advanced rendering engines. As for the artifacts, it's possible that the



Fig. 11. **Generalizing to Real-Lighting.** We reconstruct some real objects and use them to create some scenes. See Sec. 5.1 for an introduction. *Bottom:* We put the reconstructed objects to different 3D scenes. Here, NeRF means the 2D instance synthesized by NeRF. The lighting details have been successfully preserved by our LighTNet. Please see the shadows caused by object-to-object interactions. Note that, LighTNet here is only trained on the 3DF-Lighting training set. We refer to the supplementary for some rendered videos.



Fig. 12. **Reconstructed 360 Scenes and Individuals.** We initially reconstruct the scenes, persons, and objects using NeRF approaches and subsequently utilize the reconstructed elements to compose new scenes. For a comprehensive view of the 360 lighting effects, please refer to the supplementary video.

“shading residual” approach, while performing better than the compared image composition variants in Fig. 7, may not fully address the issue of uneven surfaces. We suggest that further investigation into techniques in super-resolution and diffusion models could address these challenges.

Rendering Speed. Presently, rendering an image using our method on a V100 GPU takes approximately 4 seconds. Thereby, our approach only support off-line rendering at this time. As a complement, training LighTNet on 3DF-Lighting requires approximately 12 hours utilizing a single V100 GPU. To speed up the rendering process, the UNet structure might be deeply revised and optimized.

Stability for Video Rendering. Another limitation is that our approach currently encounters stability issues in video rendering, as we have focused solely on rendering static images in this paper. To quantitatively evaluate stability, we constructed a 360-degree test set using six furniture shapes

and twelve 3D scenes from 3D-FRONT. Initially, we pre-defined a light source and energy for each scene, randomly rendering 200 images from viewpoints sampled on a full sphere to train NeRF and extract its R3DM. Subsequently, we placed the object’s R3DM into the scene, generated a random light source and energy for each 3D scene, and rendered 100 \mathcal{S}' and \mathcal{M} from viewpoints uniformly sampled on a semi-sphere around the object’s R3DM. Simultaneously, we synthesized the corresponding 100 \mathcal{I}_s using its NeRF. Finally, we rendered the 100 $\tilde{\mathcal{I}}_t$ (ground-truth images) at size 800×800 by replacing the R3DM with its 3DM. Through this workflow, we constructed a 360-degree test set with 600 samples ($\mathcal{I}_s, \mathcal{S}', \tilde{\mathcal{I}}_t, \mathcal{M}$). As reported in Table 4, although LighTNet outperforms Pix2Pix [75] in all metrics, the variances of $L1$ -Norm and PSNR are larger than Pix2Pix [75]. It makes sense since the final rendering of Pix2Pix consistently contains weak lighting effects. Modeling the temporal consistency for LighTNet would be a promising avenue for future research to overcome this limitation.



Fig. 13. **Failure Case.** One of the major limitations of LightTNet is it cannot handle strong specular materials. The reflected content would be incorrectly maintained during the rendering process. Zoom in for a better view.

TABLE 4
Stability for Video Rendering.

Metric	Pix2Pix [75]	LightTNet
L1-Norm ↓	0.0366 ± 0.0081	0.0275 ± 0.0097
PSNR ↑	27.5716 ± 1.4850	31.7297 ± 1.9355
SSIM ↑	0.9167 ± 0.0168	0.9356 ± 0.0103
Lab Angle ↓	0.4503 ± 0.0197	0.3275 ± 0.0114

8 CONCLUSION

In this paper, we are prudent to rethink reconstructed rough 3D models (R3DMs) and present a lighting transfer avenue to flexibly integrate R3DMs into practical 3D modeling workflows such as 3D scene creation, lighting editing, and rendering. Physically-based rendering (PBR) would render low-quality images of scenes constructed by R3DMs. A remedy is to represent real-world objects as individual neural fields (e.g. NeRF) in addition to R3DMs, as neural fields rendering (NFR) can synthesize photo-realistic object images under desired viewpoints. The main question is that NFR instances cannot reflect the lighting details on R3DMs. We thus present a lighting transfer network (LightTNet) as a solution. LightTNet reasons about a reformulated image composition model and can bridge the lighting gaps between NFR and PBR, such that they can benefit from each other. Moreover, we introduce a new *Lab* angle loss to enhance the contrast between lighting strength and colors. Qualitative and quantitative comparisons show the superiority of LightTNet in preserving both direct and indirect lighting effects.

REFERENCES

- [1] Q. Xu, W. Wang, D. Ceylan, R. Mech, and U. Neumann, "Disn: Deep implicit surface network for high-quality single-view 3d reconstruction," *arXiv preprint arXiv:1905.10711*, 2019.
- [2] L. Mescheder, M. Oechsle, M. Niemeyer, S. Nowozin, and A. Geiger, "Occupancy networks: Learning 3d reconstruction in function space," in *CVPR*, 2019, pp. 4460–4470.
- [3] P.-H. Huang, K. Matzen, J. Kopf, N. Ahuja, and J.-B. Huang, "Deepmvs: Learning multi-view stereopsis," in *Proceedings of the IEEE Conference on Computer Vision and Pattern Recognition*, 2018, pp. 2821–2830.
- [4] M. Niemeyer, L. Mescheder, M. Oechsle, and A. Geiger, "Differentiable volumetric rendering: Learning implicit 3d representations without 3d supervision," in *Proceedings of the IEEE/CVF Conference on Computer Vision and Pattern Recognition*, 2020, pp. 3504–3515.
- [5] L. Yariv, Y. Kasten, D. Moran, M. Galun, M. Atzmon, R. Basri, and Y. Lipman, "Multiview neural surface reconstruction by disentangling geometry and appearance," *arXiv preprint arXiv:2003.09852*, 2020.
- [6] B. Mildenhall, P. P. Srinivasan, M. Tancik, J. T. Barron, R. Ramamoorthi, and R. Ng, "Nerf: Representing scenes as neural radiance fields for view synthesis," in *European Conference on Computer Vision*. Springer, 2020, pp. 405–421.
- [7] M. Oechsle, M. Niemeyer, C. Reiser, L. Mescheder, T. Strauss, and A. Geiger, "Learning implicit surface light fields," in *3DV*. IEEE, 2020, pp. 452–462.
- [8] X. Zhang, S. Fanello, Y.-T. Tsai, T. Sun, T. Xue, R. Pandey, S. Orts-Escolano, P. Davidson, C. Rhemann, P. Debevec *et al.*, "Neural light transport for relighting and view synthesis," *ACM Transactions on Graphics (TOG)*, vol. 40, no. 1, pp. 1–17, 2021.
- [9] S. Bi, Z. Xu, P. Srinivasan, B. Mildenhall, K. Sunkavalli, M. Hašan, Y. Hold-Geoffroy, D. Kriegman, and R. Ramamoorthi, "Neural reflectance fields for appearance acquisition," *arXiv preprint arXiv:2008.03824*, 2020.
- [10] J. Thies, M. Zollhöfer, and M. Nießner, "Deferred neural rendering: Image synthesis using neural textures," *ACM Transactions on Graphics (TOG)*, vol. 38, no. 4, pp. 1–12, 2019.
- [11] K. Zhang, F. Luan, Q. Wang, K. Bala, and N. Snavely, "Physg: Inverse rendering with spherical gaussians for physics-based material editing and relighting," in *The IEEE/CVF Conference on Computer Vision and Pattern Recognition (CVPR)*, 2021.
- [12] X. Zhang, P. P. Srinivasan, B. Deng, P. Debevec, W. T. Freeman, and J. T. Barron, "NeRFactor: Neural Factorization of Shape and Reflectance Under an Unknown Illumination," *arXiv preprint arXiv:2106.01970*, 2021.
- [13] Chaosgroup, "V-ray render elements," https://docs.chaos.com/display/VMAX/RGB_Color.
- [14] A. M. Andrew, "Multiple view geometry in computer vision," *Kybernetes*, 2001.
- [15] J. L. Schönberger and J.-M. Frahm, "Structure-from-motion revisited," in *Conference on Computer Vision and Pattern Recognition (CVPR)*, 2016.
- [16] J. L. Schönberger, E. Zheng, M. Pollefeys, and J.-M. Frahm, "Pixelwise view selection for unstructured multi-view stereo," in *European Conference on Computer Vision (ECCV)*, 2016.
- [17] P. Achlioptas, O. Diamanti, I. Mitliagkas, and L. Guibas, "Learning representations and generative models for 3d point clouds," in *ICML*. PMLR, 2018, pp. 40–49.
- [18] H. Fan, H. Su, and L. J. Guibas, "A point set generation network for 3d object reconstruction from a single image," in *CVPR*, 2017, pp. 605–613.
- [19] H. Thomas, C. R. Qi, J.-E. Deschard, B. Marcotegui, F. Goulette, and L. J. Guibas, "Kpconv: Flexible and deformable convolution for point clouds," in *ICCV*, 2019, pp. 6411–6420.
- [20] G. Yang, X. Huang, Z. Hao, M.-Y. Liu, S. Belongie, and B. Hariharan, "Pointflow: 3d point cloud generation with continuous normalizing flows," in *ICCV*, 2019, pp. 4541–4550.
- [21] A. Brock, T. Lim, J. M. Ritchie, and N. Weston, "Generative and discriminative voxel modeling with convolutional neural networks," *arXiv preprint arXiv:1608.04236*, 2016.
- [22] C. B. Choy, D. Xu, J. Gwak, K. Chen, and S. Savarese, "3d-r2n2: A unified approach for single and multi-view 3d object reconstruction," in *ECCV*. Springer, 2016, pp. 628–644.
- [23] M. Gadelha, S. Maji, and R. Wang, "3d shape induction from 2d views of multiple objects," in *3DV*. IEEE, 2017, pp. 402–411.
- [24] H. Xie, H. Yao, X. Sun, S. Zhou, and S. Zhang, "Pix2vox: Context-aware 3d reconstruction from single and multi-view images," in *ICCV*, 2019, pp. 2690–2698.
- [25] J. Wu, C. Zhang, T. Xue, W. T. Freeman, and J. B. Tenenbaum, "Learning a probabilistic latent space of object shapes via 3d generative-adversarial modeling," in *NeurIPS*, 2016, pp. 82–90.
- [26] A. Kanazawa, S. Tulsiani, A. A. Efros, and J. Malik, "Learning category-specific mesh reconstruction from image collections," in *ECCV*, 2018, pp. 371–386.
- [27] Y. Liao, S. Donne, and A. Geiger, "Deep marching cubes: Learning explicit surface representations," in *CVPR*, 2018, pp. 2916–2925.
- [28] J. Pan, X. Han, W. Chen, J. Tang, and K. Jia, "Deep mesh reconstruction from single rgb images via topology modification networks," in *Proceedings of the IEEE/CVF International Conference on Computer Vision*, 2019, pp. 9964–9973.

- [29] N. Wang, Y. Zhang, Z. Li, Y. Fu, W. Liu, and Y.-G. Jiang, "Pixel2mesh: Generating 3d mesh models from single rgb images," in *ECCV*, 2018, pp. 52–67.
- [30] M. Atzmon, N. Haim, L. Yariv, O. Israelov, H. Maron, and Y. Lipman, "Controlling neural level sets," *arXiv preprint arXiv:1905.11911*, 2019.
- [31] S. Saito, Z. Huang, R. Natsume, S. Morishima, A. Kanazawa, and H. Li, "Pifu: Pixel-aligned implicit function for high-resolution clothed human digitization," in *ICCV*, 2019, pp. 2304–2314.
- [32] J. J. Park, P. Florence, J. Straub, R. Newcombe, and S. Lovegrove, "DeepSDF: Learning continuous signed distance functions for shape representation," in *CVPR*, 2019, pp. 165–174.
- [33] M. Michalkiewicz, J. K. Pontes, D. Jack, M. Baktashmotlagh, and A. Eriksson, "Implicit surface representations as layers in neural networks," in *ICCV*, 2019, pp. 4743–4752.
- [34] P. Wang, L. Liu, Y. Liu, C. Theobalt, T. Komura, and W. Wang, "Neus: Learning neural implicit surfaces by volume rendering for multi-view reconstruction," *arXiv preprint arXiv:2106.10689*, 2021.
- [35] M. Oechsle, S. Peng, and A. Geiger, "Unisurf: Unifying neural implicit surfaces and radiance fields for multi-view reconstruction," in *Proceedings of the IEEE/CVF International Conference on Computer Vision*, 2021, pp. 5589–5599.
- [36] L. Yariv, J. Gu, Y. Kasten, and Y. Lipman, "Volume rendering of neural implicit surfaces," *Advances in Neural Information Processing Systems*, vol. 34, 2021.
- [37] Z. Chen, T. Funkhouser, P. Hedman, and A. Tagliasacchi, "Mobilerf: Exploiting the polygon rasterization pipeline for efficient neural field rendering on mobile architectures," *arXiv preprint arXiv:2208.00277*, 2022.
- [38] Meta, "Meta connect 2022," <https://www.youtube.com/watch?v=hvf59iGwYX8>.
- [39] R. Martin-Brualla, N. Radwan, M. S. Sajjadi, J. T. Barron, A. Dosovitskiy, and D. Duckworth, "Nerf in the wild: Neural radiance fields for unconstrained photo collections," in *CVPR*, 2021, pp. 7210–7219.
- [40] T. Neff, P. Stadlbauer, M. Parger, A. Kurz, C. R. A. Chaitanya, A. Kaplanyan, and M. Steinberger, "Donerf: Towards real-time rendering of neural radiance fields using depth oracle networks," *arXiv preprint arXiv:2103.03231*, 2021.
- [41] M. Niemeyer and A. Geiger, "Giraffe: Representing scenes as compositional generative neural feature fields," *arXiv preprint arXiv:2011.12100*, 2020.
- [42] S. Peng, Y. Zhang, Y. Xu, Q. Wang, Q. Shuai, H. Bao, and X. Zhou, "Neural body: Implicit neural representations with structured latent codes for novel view synthesis of dynamic humans," in *CVPR*, 2021, pp. 9054–9063.
- [43] A. Pumarola, E. Corona, G. Pons-Moll, and F. Moreno-Noguer, "D-nerf: Neural radiance fields for dynamic scenes," *arXiv preprint arXiv:2011.13961*, 2020.
- [44] K. Zhang, G. Riegler, N. Snavely, and V. Koltun, "Nerf++: Analyzing and improving neural radiance fields," *arXiv preprint arXiv:2010.07492*, 2020.
- [45] M. Suhail, C. Esteves, L. Sigal, and A. Makadia, "Light field neural rendering," in *Proceedings of the IEEE/CVF Conference on Computer Vision and Pattern Recognition (CVPR)*, June 2022, pp. 8269–8279.
- [46] J. T. Barron, B. Mildenhall, M. Tancik, P. Hedman, R. Martin-Brualla, and P. P. Srinivasan, "Mip-nerf: A multiscale representation for anti-aliasing neural radiance fields," in *Proceedings of the IEEE/CVF International Conference on Computer Vision (ICCV)*, October 2021, pp. 5855–5864.
- [47] A. Yu, R. Li, M. Tancik, H. Li, R. Ng, and A. Kanazawa, "PlenOc-trees for real-time rendering of neural radiance fields," in *ICCV*, 2021.
- [48] C. Sun, M. Sun, and H.-T. Chen, "Direct voxel grid optimization: Super-fast convergence for radiance fields reconstruction," in *Proceedings of the IEEE/CVF Conference on Computer Vision and Pattern Recognition (CVPR)*, June 2022, pp. 5459–5469.
- [49] A. Chen, Z. Xu, A. Geiger, J. Yu, and H. Su, "Tensorf: Tensorial radiance fields," in *European Conference on Computer Vision (ECCV)*, 2022.
- [50] T. Hu, S. Liu, Y. Chen, T. Shen, and J. Jia, "Efficientnerf efficient neural radiance fields," in *Proceedings of the IEEE/CVF Conference on Computer Vision and Pattern Recognition (CVPR)*, June 2022, pp. 12 902–12 911.
- [51] J. T. Barron, B. Mildenhall, D. Verbin, P. P. Srinivasan, and P. Hedman, "Mip-nerf 360: Unbounded anti-aliased neural radiance fields," in *Proceedings of the IEEE/CVF Conference on Computer Vision and Pattern Recognition (CVPR)*, June 2022, pp. 5470–5479.
- [52] D. Verbin, P. Hedman, B. Mildenhall, T. Zickler, J. T. Barron, and P. P. Srinivasan, "Ref-nerf: Structured view-dependent appearance for neural radiance fields," in *Proceedings of the IEEE/CVF Conference on Computer Vision and Pattern Recognition (CVPR)*, June 2022, pp. 5491–5500.
- [53] J. Philip, S. Morgenthaler, M. Gharbi, and G. Drettakis, "Free-viewpoint indoor neural relighting from multi-view stereo," *ACM Transactions on Graphics (TOG)*, vol. 40, no. 5, pp. 1–18, 2021.
- [54] W. Ye, S. Chen, C. Bao, H. Bao, M. Pollefeys, Z. Cui, and G. Zhang, "Intrinsicnerf: Learning intrinsic neural radiance fields for editable novel view synthesis," *arXiv preprint arXiv:2210.00647*, 2022.
- [55] M. Tancik, V. Casser, X. Yan, S. Pradhan, B. Mildenhall, P. P. Srinivasan, J. T. Barron, and H. Kretzschmar, "Block-nerf: Scalable large scene neural view synthesis," in *Proceedings of the IEEE/CVF Conference on Computer Vision and Pattern Recognition*, 2022, pp. 8248–8258.
- [56] X. Zhang, P. P. Srinivasan, B. Deng, P. Debevec, W. T. Freeman, and J. T. Barron, "Nerfactor: Neural factorization of shape and reflectance under an unknown illumination," *arXiv preprint arXiv:2106.01970*, 2021.
- [57] M. Boss, R. Braun, V. Jampani, J. T. Barron, C. Liu, and H. Lensch, "Nerd: Neural reflectance decomposition from image collections," *arXiv preprint arXiv:2012.03918*, 2020.
- [58] P. P. Srinivasan, B. Deng, X. Zhang, M. Tancik, B. Mildenhall, and J. T. Barron, "Nerv: Neural reflectance and visibility fields for relighting and view synthesis," *arXiv preprint arXiv:2012.03927*, 2020.
- [59] Y. Zhang, J. Sun, X. He, H. Fu, R. Jia, and X. Zhou, "Modeling indirect illumination for inverse rendering," in *Proceedings of the IEEE/CVF Conference on Computer Vision and Pattern Recognition*, 2022, pp. 18 643–18 652.
- [60] M. Janner, J. Wu, T. D. Kulkarni, I. Yildirim, and J. B. Tenenbaum, "Self-supervised intrinsic image decomposition," in *NeurIPS*, 2017, pp. 5938–5948.
- [61] W.-C. Ma, H. Chu, B. Zhou, R. Urtasun, and A. Torralba, "Single image intrinsic decomposition without a single intrinsic image," in *ECCV*, 2018, pp. 201–217.
- [62] H. Zhou, X. Yu, and D. W. Jacobs, "Glosh: Global-local spherical harmonics for intrinsic image decomposition," in *Proceedings of the IEEE/CVF International Conference on Computer Vision*, 2019, pp. 7820–7829.
- [63] Y. Liu, Y. Li, S. You, and F. Lu, "Unsupervised learning for intrinsic image decomposition from a single image," in *Proceedings of the IEEE/CVF Conference on Computer Vision and Pattern Recognition*, 2020, pp. 3248–3257.
- [64] J. T. Kajiya, "The rendering equation," in *Proceedings of the 13th annual conference on Computer graphics and interactive techniques*, 1986, pp. 143–150.
- [65] Blender, <https://www.blender.org>.
- [66] S. Sengupta, A. Kanazawa, C. D. Castillo, and D. W. Jacobs, "Sfsnet: Learning shape, reflectance and illuminance of faces in the wild," in *Proceedings of the IEEE conference on computer vision and pattern recognition*, 2018, pp. 6296–6305.
- [67] Y. Yu and W. A. Smith, "Inverserendernet: Learning single image inverse rendering," in *Proceedings of the IEEE/CVF Conference on Computer Vision and Pattern Recognition*, 2019, pp. 3155–3164.
- [68] Z. Li, Z. Xu, R. Ramamoorthi, K. Sunkavalli, and M. Chandraker, "Learning to reconstruct shape and spatially-varying reflectance from a single image," *ACM Transactions on Graphics (TOG)*, vol. 37, no. 6, pp. 1–11, 2018.
- [69] J. Johnson, A. Alahi, and L. Fei-Fei, "Perceptual losses for real-time style transfer and super-resolution," in *European conference on computer vision*. Springer, 2016, pp. 694–711.
- [70] K. Simonyan and A. Zisserman, "Very deep convolutional networks for large-scale image recognition," *arXiv preprint arXiv:1409.1556*, 2014.
- [71] J. Deng, W. Dong, R. Socher, L.-J. Li, K. Li, and L. Fei-Fei, "Imagenet: A large-scale hierarchical image database," in *2009 IEEE conference on computer vision and pattern recognition*. Ieee, 2009, pp. 248–255.
- [72] Z. Wang, A. C. Bovik, H. R. Sheikh, and E. P. Simoncelli, "Image quality assessment: from error visibility to structural similarity," *IEEE transactions on image processing*, vol. 13, no. 4, pp. 600–612, 2004.

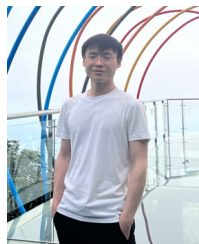
- [73] T. Nestmeyer, J.-F. Lalonde, I. Matthews, and A. Lehrmann, "Learning physics-guided face relighting under directional light," in *Proceedings of the IEEE/CVF Conference on Computer Vision and Pattern Recognition*, 2020, pp. 5124–5133.
- [74] K. Nazeri, E. Ng, T. Joseph, F. Z. Qureshi, and M. Ebrahimi, "Edgeconnect: Generative image inpainting with adversarial edge learning," *arXiv preprint arXiv:1901.00212*, 2019.
- [75] P. Isola, J.-Y. Zhu, T. Zhou, and A. A. Efros, "Image-to-image translation with conditional adversarial networks," in *Proceedings of the IEEE conference on computer vision and pattern recognition*, 2017, pp. 1125–1134.
- [76] H. Zhou, S. Hadap, K. Sunkavalli, and D. W. Jacobs, "Deep single-image portrait relighting," in *Proceedings of the IEEE/CVF International Conference on Computer Vision*, 2019, pp. 7194–7202.
- [77] H. Fu, B. Cai, L. Gao, L.-X. Zhang, J. Wang, C. Li, Q. Zeng, C. Sun, R. Jia, B. Zhao *et al.*, "3d-front: 3d furnished rooms with layouts and semantics," in *Proceedings of the IEEE/CVF International Conference on Computer Vision*, 2021, pp. 10 933–10 942.
- [78] C. Loop, "Smooth subdivision surfaces based on triangles," Master's thesis, Department of Mathematics, University of Utah, 1987.
- [79] Q.-Y. Zhou, J. Park, and V. Koltun, "Open3D: A modern library for 3D data processing," *arXiv:1801.09847*, 2018.
- [80] M. Işık, M. Rünz, M. Georgopoulos, T. Khakhulin, J. Starck, L. Agapito, and M. Nießner, "Humanrf: High-fidelity neural radiance fields for humans in motion," *ACM Transactions on Graphics (TOG)*, vol. 42, no. 4, pp. 1–12, 2023. [Online]. Available: <https://doi.org/10.1145/3592415>
- [81] T. Müller, A. Evans, C. Schied, and A. Keller, "Instant neural graphics primitives with a multiresolution hash encoding," *ACM Transactions on Graphics (ToG)*, vol. 41, no. 4, pp. 1–15, 2022.



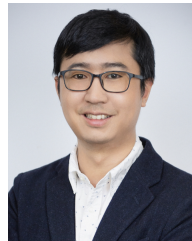
Rongfei Jia is a Staff Algorithm Expert at Tao Technology Department, Alibaba Group. He received his PhD degree from Beihang University. He is leading an algorithm team which is devoted in 3D AI modeling and generation technologies. His research interests include 3D object modeling, scene understanding and synthesis.



Bingqiang Zhao was a Senior Staff Algorithm Expert at Tao Technology Department, Alibaba Group. He graduated from Tsinghua University in 2006. He was the head of Taobao Business Machine Intelligence Department.



Bowen Cai is an Algorithm Expert at Tao Technology Department, Alibaba Group. He received his PhD degree from Beihang University. After that, he was a postdoctoral researcher, working with Prof. Hua Li at the Institute of Computing Technology, Chinese Academy of Sciences and Yinghui Xu at Alibaba Group. His interests include semantic segmentation, 3D reconstruction, and neural rendering.



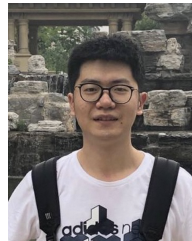
Mingming Gong is a Senior Lecturer in data science with the School of Mathematics and Statistics, the University of Melbourne. He has authored and co-authored 60+ research papers on top venues such as ICML, NeurIPS, ICLR, CVPR, TPAMI, and IJCV with 10+ oral/spotlight presentations. He received the Discovery Early Career Researcher Award from Australian Research Council in 2021. His research interests include causal reasoning, machine learning, and computer vision.



Yujie Li was an Algorithm Engineer at Tao Technology Department, Alibaba Group. She received her master degree from Beijing University of Technology, in 2020. She currently works on 3D scene synthesis and neural rendering.



Yuqing Liang is an Algorithm Engineer at Tao Technology Department, Alibaba Group. He received her master degree from Najing University, in 2022. He currently works on 3D reconstruction and neural rendering.



Huan Fu is a Staff Algorithm Expert at Tao Technology Department, Alibaba Group. He received the BSc degree from University of Science and Technology of China, in 2014, and the PhD degree from The University of Sydney, Australia, in 2019. He has authored and co-authored 20+ research papers on top venues such as NeurIPS, CVPR, ICCV, IJCV, and TPAMI, with a best paper finalist in CVPR19. His research interests include 2D/3D scene understanding, 3D reconstruction, and neural rendering.

SUPPLEMENTARY MATERIAL

CONTENTS

The supplementary materials consist of:

- The detailed network architectures.
- Two videos that records that an artist designs some rooms via R3DMs and R3Ds and renders high-quality images or videos leveraging LighTNet.
- More qualitative results (images and videos).

S1 NETWORK ARCHITECTURES

The network architectures for the lighting transfer network (LighTNet) are reported in S.Figure S1. For convenience, we use the following abbreviation: C_{in} = Input Channel, C_{out} = Feature Channel, K = Kernel Size, S = Stride Size, Conv2D = Convolutional Layer.

S2 MORE QUALITATIVE RESULTS

S.Figure S2 provides more qualitative comparisons on the 3DF-Lighting test set. In S.Figure S3-S5 and the supplemental video, we incorporate more rendered results of scenes created by R3DMs of real objects (See "Generalizing to Real-Lighting" in the main paper).

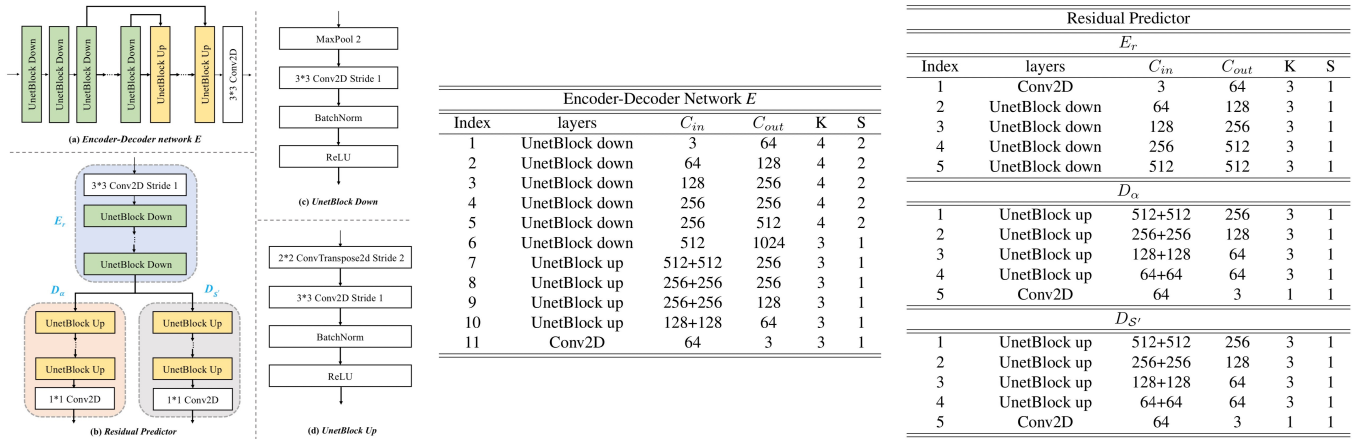


Fig. S1. **Network Architecture.** (a). Encoder-Decoder Network E . (b). Residual Predictor. D_α and $D_{S'}$ share the same encoder E_r , and are used to estimate the residual lighting effect α and shading S' , respectively. (c). The U-Net downsampling block in E and E_r . (d). The U-Net upsampling block in E , D_α and $D_{S'}$. Zoom in for a better view.



Fig. S2. More qualitative comparisons with baseline methods on the 3DF-Lighting test set. LightNet can well preserve the lighting details (e.g., local shadows.) Zoom in for a better view.

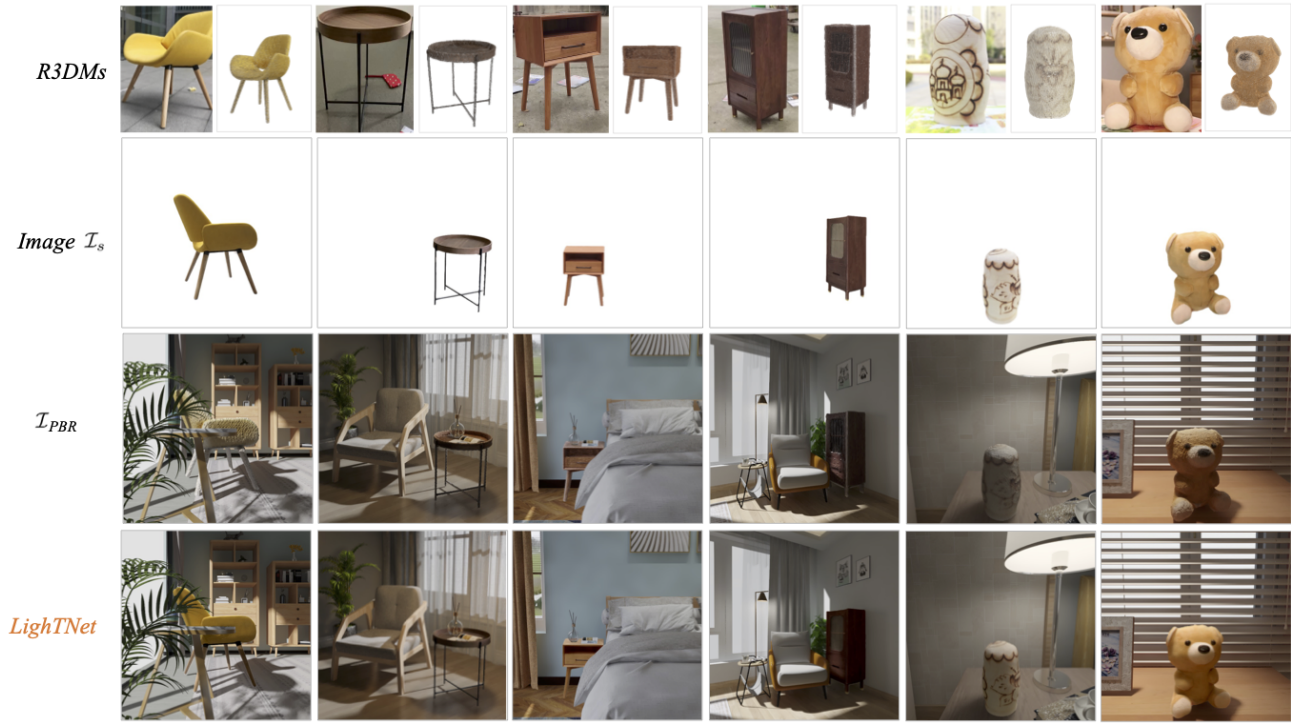


Fig. S3. More rendered results of scenes created by R3DMs of real objects. Zoom in for a better view.

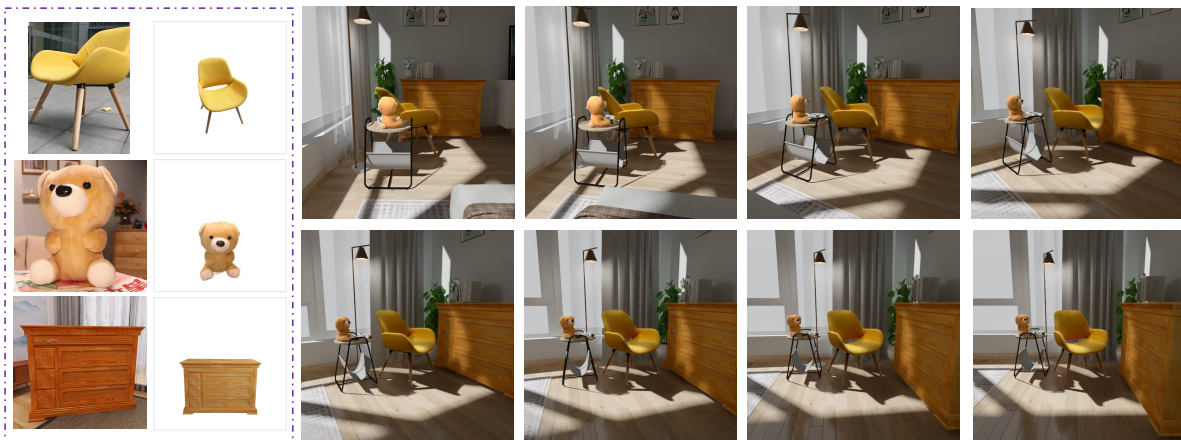


Fig. S4. The R3DMs including bear, chair, and cabinet are put into room to make it collaborate with other 3D CAD furniture. Their lightings are transferred by LighTNet, while other 3D CAD models are rendered by PBR. We can see that R3DMs transferred by LighTNet can be well compatible with the PBR scene. Zoom in for a better view.

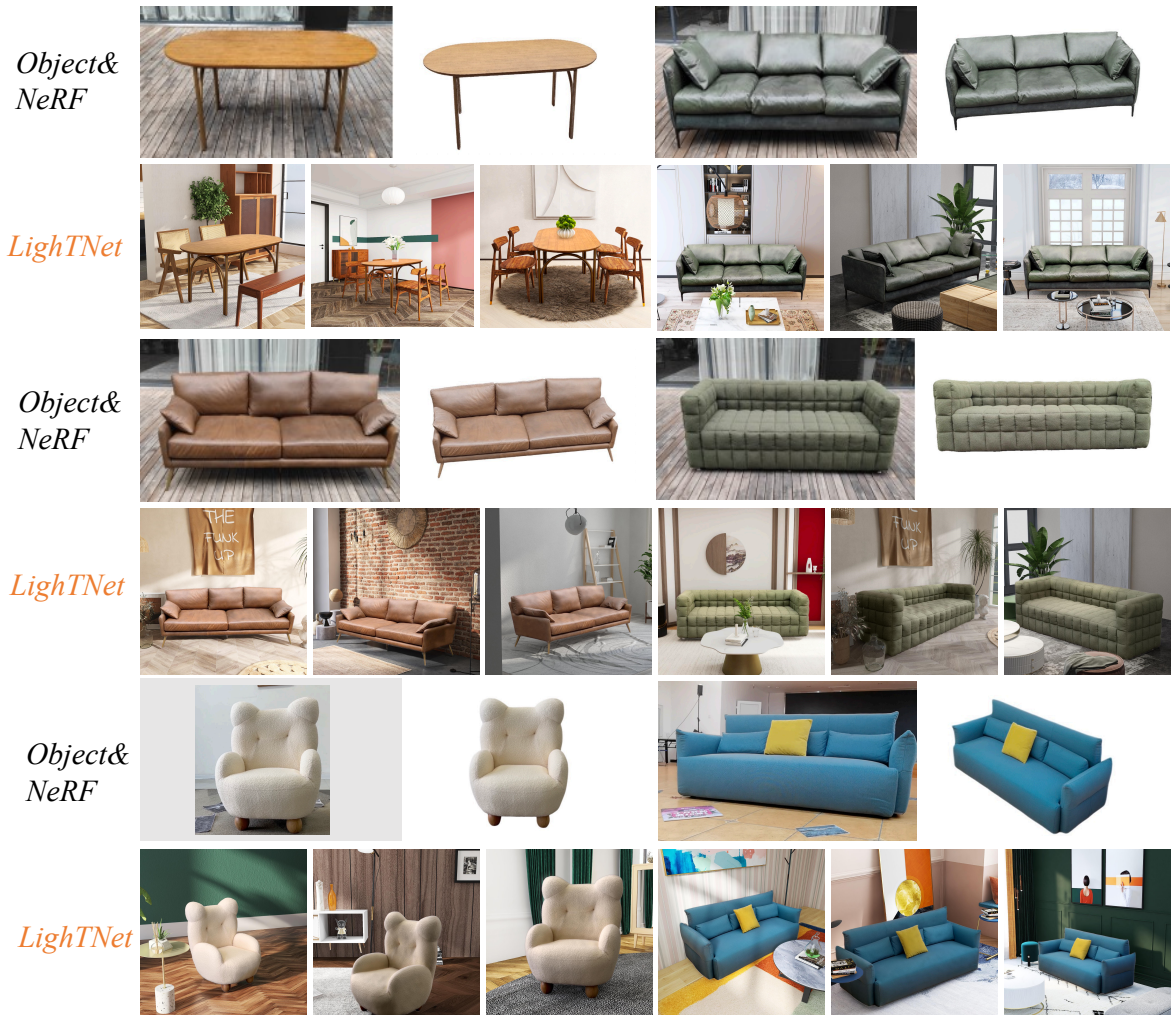


Fig. S5. We put the reconstructed objects to different 3D scenes. Here, NeRF means the 2D instance synthesized by NeRF. The lighting details have been successfully preserved by our LighTNet approach.